Nonlinear Maximum Power Point Tracking Control and Modal Analysis of DFIG Based Wind Turbine

B. Yang, L. Jiang, *Member, IEEE*, L. Wang, Q. H. Wu, *Fellow, IEEE*

***Abstract*—The doubly fed induction generator based wind turbine (DFIG-WT) has strong nonlinearities originated from the aerodynamics of wind turbine and the coupled dynamic of the DFIG and can operate under a time-varying and wide operation region. Based on the detailed model of DFIG-WT, a feedback linearization controller is designed in this paper to achieve the maximize the captured wind energy in the variable speed operation range, by which fully decoupled control of the external dynamics is achieved and the stability of remained internal dynamics is analyzed in the sense of Lyapunov. Moreover, modal analysis is employed to verify the consistent dynamic under different operation conditions and low-voltage ride-through (LVRT) capability provided by the proposed nonlinear controller. Simulation study verifies that more accurate tracking and superior LVRT capability can be achieved in comparison with conventional vector control (VC).**

***Index Terms*—DFIG-WT, nonlinear control, modal analysis, MPPT, internal dynamics stability, low-voltage ride-through**

I. Introduction

Nowadays doubly-fed induction generator based wind turbines (DFIG-WTs) have been one popular wind power generation system and widely installed in industry due to their merits of high energy conversion efficiency from variable speed operation and relative low-cost of power electronic converter [1]. The performance of DFIG-WTs fully depends upon control systems applied on turbine side and generator side which are generally designed via a cascade structure way including a fast inner-loop for power control of the DFIG and a slow outer-loop for speed control of the drive-train of DFIG-WT. Wind turbine also utilizes pitch angle control to adjust the output power for wind speed above the rated speed. Below the rated wind speed, one of the crucial control task is to maximize the captured wind energy via variable speed operation, which requires the DFIG-WT must be fully controllable and operated at an optimal rotor speed according to time-varying wind speed, simultaneously minimizing the driven-train mechanical load [2].

In the past decade, modeling and control of DFIG-WT have attracted extensive research efforts [3]. Among those results, vector control (VC) with proportional-integral (PI) loops is the most used control algorithm for the power regulation of the DFIG, due to the capability of decoupling control of active/reactive power and simple structure [4]. This approach is generally derived based on two basic assumptions, namely the constant stator flux or stator voltage, and negligible stator resistance [5]–[7]. However, the stator flux and stator voltage is no longer constant under grid faults or load variations. Moreover, the presence of small stator resistance will result in a poorly damped dynamics of stator flux. On the other hand, the dynamic of of VC relies on the fine tuning of gains of proportional-integral (PI) controllers. Although the suitable range can be found via the observation of each mode loci using modal analysis [8], unsuitable control gains may result in Hopf bifurcation [9]. Their optimal parameters can be determined by other methods such as particle swarm optimization [10]. However, the optimal parameters obtained merely corresponded to one specific operation point, while cannot provide global consistent performance as the operation points of DFIG-WT varies with the wind power inputs.

In fact, the DFIG-WT has strong nonlinearities originated from the aerodynamics of wind turbine and the coupled dynamic of the DFIG and operates under a time-varying and wide operation region according to turbulent wind power inputs. To tackle this issue, nonlinear control methodologies have been applied, such as a wind speed estimator based nonlinear static and dynamic state feedback controller for variable speed wind turbine [11], a sliding mode controller for power extraction and regulation under model uncertainties [12], a nonlinear back-stepping approach for achieving optimal reference tracking and globally asymptotically stable in the context of Lyapunov theory [13], and feedback linearization control (FLC) [14]–[16]. FLC compensates system nonlinearities through exact linearization and controlling of the equivalent linear system so as to provide a global optimal control performance across the whole operation region. A FLC approach was systematically developed in [14] for high-performance control of AC/DC PWM converters, and a decentralized nonlinear controller is designed in the transient stability control of power systems based on a third-order DFIG-WT model [15]. In order to reject the effect of the external disturbances, [16] proposes a feedback linearization controller equipped with a disturbance observer for the estimation of parameter uncertainties.

As a consequence, those assumptions of the VC are removed as all system dynamics are considered and the tuning load of control gains are reduced. Moreover, controller is designed in an integrated way comparing with the cascade-structure of the VC. To achieve the fully linearization, some work ignored the stator dynamic and used third-order system model. Nevertheless, due to this model simplification, the stator dynamics were ignored, and the system transient dynamics was lost.

B. Yang, L. Jiang, L. Wang and Q. H. Wu are with the Department of Electrical Engineering & Electronics, University of Liverpool, Liverpool, L69 3GJ, UK. (Email: yangbo@liv.ac.uk, ljiang@liv.ac.uk, lwang@liv.ac.uk, qhwu@liv.ac.uk)

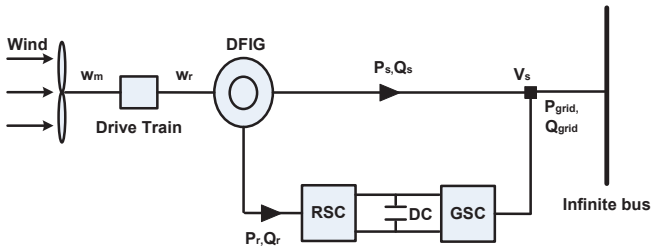

Fig. 1. The configuration of the grid connected DFIG-WT.

However, when the system relative degree is less than system order the internal dynamics will emerge, which stability is unclear during the FLC design. In fact numerous examples have shown that the unstable internal dynamics can lead to the unbounded output [17], therefore it must be analyzed particularly.

Since the system nonlinearity is fully removed by FLC a global optimal control can be achieved. This paper designs a feedback linearization controller based on the detailed DFIG-WT model to achieve MPPT, therefore the stator dynamics is included and the internal dynamics is proven to be stable in the sense of Lyapunov. We use both the modal analysis and simulation study to show the system LVRT capacity and parameter robustness, which provides a new perspective to these issues.

The remaining of the paper is organized as follows. Section II is devoted to the basic development of DFIG-WT model. Section III presents the nonlinear control design of rotor side converter (RSC), which is further divided into two parts, i.e., imposing the desired external dynamics of the model on the one hand, and the analysis of the internal dynamics stability on the other. In Section IV both the modal analysis and simulation study are carried out to verify the effectiveness of our proposed approach. Finally, Section V completes the paper and reports the most meaningful conclusions extracted.

II. Dynamic Model of DFIG-WT

A schematic diagram of DFIG-WT is shown in Fig. 1. The wind turbine is connected to the induction generator through a mechanical shaft system. And the stator is directly connected to grid while rotor is fed through a back-to-back converter.

A. Wind turbine aerodynamic model

The aerodynamic model of a wind turbine can be characterized by the energy conversion coefficient $C_{\rm p}(\lambda,\beta)$, which is a function of both tip-speed-ratio λ and blade pitch angle β, in which λ is defined by

$$\lambda = \frac{w_{\rm m} R}{v_{\rm wind}} \tag{1}$$

where R is the blade radius, $\omega_{\rm m}$ is the wind turbine rotational speed and $v_{\rm wind}$ is the wind speed. Based on the wind turbine characteristics, a generic equation used to model $C_{\rm p}(\lambda,\beta)$ is [8]

$$C_{\rm p}(\lambda,\beta) = c_1\left(\frac{c_2}{\lambda_i} - c_3\beta - c_4\right)e^{-\frac{c_5}{\lambda_i}} + c_6\lambda \tag{2}$$

with

$$\frac{1}{\lambda_i} = \frac{1}{\lambda + 0.08\beta} - \frac{0.035}{\beta^3 + 1} \tag{3}$$

The coefficients c_1 to c_6 are: c_1=0.5176, c_2=116, c_3=0.4, c_4=5, c_5=21 and c_6=0.0068 [20].

The mechanical power that wind turbine extracts from the wind is calculated as

$$P_{\rm m} = \frac{1}{2}\rho\pi R^2 C_{\rm p}(\lambda,\beta) v_{\rm wind}^3 \tag{4}$$

where ρ is the air density. We consider the wind turbine operates in the sub-rated speed range hence its pitch control is deactivated such that $\beta \equiv 0$.

B. Generator model

The induction generator used is a single-cage wound rotor induction machine. The dynamics of the system can be modeled by a set of differential algebraic equations in per unit on machine base. We define $e'_{\rm qs} = (L_{\rm m}/L_{\rm rr})w_{\rm s}\psi_{\rm dr}$, $e'_{\rm ds} = -(L_{\rm m}/L_{\rm rr})w_{\rm s}\psi_{\rm qr}$, $L'_{\rm s} = L_{\rm ss} - L_{\rm m}^2/L_{\rm rr}$, $T_{\rm r} = L_{\rm rr}/R_{\rm r}$, $R_1 = R_{\rm s} + R_2$ and $R_2 = (L_{\rm m}/L_{\rm rr})^2 R_{\rm r}$. After some substitutions and rearrangements the generator dynamics are described as followed [8]:

$$\begin{aligned}\frac{di_{\rm qs}}{dt} =& \frac{\omega_{\rm b}}{L'_{\rm s}}\Big(-R_1 i_{\rm qs} + \omega_{\rm s} L'_{\rm s} i_{\rm ds} + \frac{\omega_{\rm r}}{\omega_{\rm s}} e'_{\rm qs} - \frac{1}{T_{\rm r}\omega_{\rm s}} e'_{\rm ds} \\ & - v_{\rm qs} + \frac{L_{\rm m}}{L_{\rm rr}} v_{\rm qr}\Big)\end{aligned} \tag{5}$$

$$\begin{aligned}\frac{di_{\rm ds}}{dt} =& \frac{\omega_{\rm b}}{L'_{\rm s}}\Big(-\omega_{\rm s} L'_{\rm s} i_{\rm qs} - R_1 i_{\rm ds} + \frac{1}{T_{\rm r}\omega_{\rm s}} e'_{\rm qs} + \frac{\omega_{\rm r}}{\omega_{\rm s}} e'_{\rm ds} \\ & - v_{\rm ds} + \frac{L_{\rm m}}{L_{\rm rr}} v_{\rm dr}\Big)\end{aligned} \tag{6}$$

$$\begin{aligned}\frac{de'_{\rm qs}}{dt} =& \omega_{\rm b}\omega_{\rm s}\Big[R_2 i_{\rm ds} - \frac{1}{T_{\rm r}\omega_{\rm s}} e'_{\rm qs} + \left(1 - \frac{\omega_{\rm r}}{\omega_{\rm s}}\right) e'_{\rm ds} \\ & - \frac{L_{\rm m}}{L_{\rm rr}} v_{\rm dr}\Big]\end{aligned} \tag{7}$$

$$\begin{aligned}\frac{de'_{\rm ds}}{dt} =& \omega_{\rm b}\omega_{\rm s}\Big[-R_2 i_{\rm qs} - \Big(1 - \frac{\omega_{\rm r}}{\omega_{\rm s}}\Big) e'_{\rm qs} - \frac{1}{T_{\rm r}\omega_{\rm s}} e'_{\rm ds} \\ & + \frac{L_{\rm m}}{L_{\rm rr}} v_{\rm qr}\Big]\end{aligned} \tag{8}$$

where $\psi_{\rm dr}$ and $\psi_{\rm qr}$ are the direct (d) and quadrature (q) axis rotor flux linkages; $R_{\rm s}$ and $R_{\rm r}$ are the stator and rotor resistances; $L_{\rm ss}$ and $L_{\rm rr}$ are the stator and rotor self-inductances; $L_{\rm m}$ is the mutual inductance; $\omega_{\rm b}$ is the electrical base speed; $\omega_{\rm s}$ is the synchronous angle speed; $T_{\rm r}$ is the rotor circuit time constant; $e'_{\rm ds}$ and $e'_{\rm qs}$ are the d and q axis voltages behind the transient; $i_{\rm ds}$ and $i_{\rm qs}$ are the d and q axis stator currents; $v_{\rm ds}$ and $v_{\rm qs}$ are the d and q axis stator terminal voltages, aligning the q-axis with stator voltage and the d-axis leading the q-axis, $v_{\rm ds}$ becomes zero and $v_{\rm qs}$ equals to the magnitude of the terminal voltage; $v_{\rm dr}$ and $v_{\rm qr}$ are the d and q axis rotor voltages, respectively.

The electromagnetic torque $T_{\rm e}$ produced by the generator is obtained as

$$T_{\rm e} = (e'_{\rm qs}/\omega_{\rm s}) i_{\rm qs} + (e'_{\rm ds}/\omega_{\rm s}) i_{\rm ds} \tag{9}$$

C. Drive train model

The drive train comprises turbine, gearbox, shafts and other mechanical components. The shaft system can be represented either by a two-mass or single lumped-mass model [18]. In the two-mass model, separate masses are used to describe the low-speed turbine and the high-speed generator, and the connecting resilient shaft is modeled as a spring and a damper [11]. As the mechanical mode is of less interest in our nonlinear controller design the lumped-mass model is chosen here.

$$\frac{d\omega_{\mathrm{m}}}{dt} = \frac{1}{2H_{\mathrm{m}}}\left(T_{\mathrm{m}} - T_{\mathrm{e}} - D\omega_{\mathrm{m}}\right) \tag{10}$$

where H_{m} is the lumped inertia constant, the rotational speed ω_{m} is equal to the rotor speed ω_{r} in the lumped-mass model, D represents the damping of the lumped system, T_{m} is the mechanical torque given as $T_{\mathrm{m}} = P_{\mathrm{m}}/w_{\mathrm{m}}$ and T_{e} is calculated from (9).

In order to harvest the maximum amount of energy from the wind, the wind turbine must be regulated at a specific rotational speed to maintain its tip-speed-ratio λ as close as possible to its optimal value λ_{opt}. This can be achieved by the adjustment of rotor speed controller such that $C_{\mathrm{p}}(\lambda,\beta)$ remains at the $C_{\mathrm{p\_max}}(\lambda,\beta)$ point [21].

III. FLC OF DFIG-WT

Feedback linearization is a typical approach in nonlinear control theory. The idea is to transform a nonlinear system dynamics into an equivalent (fully or partly) linear one through a change of state variables and a suitable nonlinear control input, so that linear control techniques can be then applied to the nonlinear system [17].

A. Multiple Input Multiple Output (MIMO) feedback linearization

We consider a standard affine MIMO system in a neighborhood around an operation point x_0 of the form

$$\begin{cases} \dot{x} = f(x) + g(x)u \\ y = h(x) \end{cases} \tag{11}$$

where $x \in R^n$ is the state vector, $u \in R^m$ is the control input vector, $y \in R^m$ is the output vector, $f(x)$, $g(x)$ and $h(x)$ are the smooth and continuous vector fields. The input-output linearisation of a MIMO system is obtained via differentiating the output y_i of the system until the input u_j appears, assuming that r_i is the smallest integer such that at least one of the inputs explicitly appears in $y_i^{(r_i)}$

$$y_i^{(r_i)} = L_f^{r_i} h_i + \sum_{j=1}^{m} L_{g_j} L_f^{r_i-1} h_i u_j \tag{12}$$

where $y_i^{(r_i)}$ denotes the i^{th}-order derivative of y_i, if $L_{g_j} L_f^{r_i-1} h_i(x) \neq 0$ for at least one j. Repeating the above procedure for each output y_i gives

$$\begin{bmatrix} y_1^{(r_1)} \\ \vdots \\ y_m^{(r_m)} \end{bmatrix} = \begin{bmatrix} L_f^{r_1} h_1 \\ \vdots \\ L_f^{r_m} h_m \end{bmatrix} + B(x) \begin{bmatrix} u_1 \\ \vdots \\ u_m \end{bmatrix} \tag{13}$$

$$B(x) = \begin{bmatrix} L_{g_1} L_f^{r_1-1} h_1 & \cdots & L_{g_m} L_f^{r_1-1} h_1 \\ \vdots & \vdots & \vdots \\ L_{g_1} L_f^{r_m-1} h_m & \cdots & L_{g_m} L_f^{r_m-1} h_m \end{bmatrix} \tag{14}$$

Here $B(x)$ is the $m \times m$ control gain matrix. Ω is defined as the intersection of the Ω_i. If the partial "relative degrees" r_i are all well defined, then Ω is itself a finite neighborhood of x_0. Furthermore, if $B(x)$ is invertible the physical control law of the MIMO nonlinear system can be derived as

$$u = B(x)^{-1}\left\{ \begin{bmatrix} -L_f^{r_1} h_1 \\ \vdots \\ -L_f^{r_m} h_m \end{bmatrix} + \begin{bmatrix} v_1 \\ \vdots \\ v_m \end{bmatrix} \right\} \tag{15}$$

where v_i is the new input of the system. Now the equivalent linear dynamics become

$$y_i^{(r_i)} = v_i \tag{16}$$

Since the input v_i only affects the output y_i this is a decoupled control law, and the invertible matrix $B(x)$ is called the decoupled matrix of the system. The transformed system is now said to have relative degree $(r_1,\ldots,r_m)$ at x_0, and we define the scalar $r = r_1 + \ldots + r_m$ as the total relative degree of the system at x_0.

B. Nonlinear MPPT control

We choose the rotor speed ω_{r} and stator reactive power Q_{s} as the outputs

$$\begin{cases} y_1 = \omega_{\mathrm{r}} \\ y_2 = Q_{\mathrm{s}} \end{cases} \tag{17}$$

and define the tracking error $e = [e_1 \;\; e_2]^T$ as

$$\begin{cases} e_1 = \omega_{\mathrm{r}} - \omega_{\mathrm{r\_ref}} \\ e_2 = Q_{\mathrm{s}} - Q_{\mathrm{s\_ref}} \end{cases} \tag{18}$$

where $\omega_{\mathrm{r\_ref}} = \lambda_{\mathrm{opt}} v_{\mathrm{wind}}/R$ and $Q_{\mathrm{s\_ref}} \equiv 0$. Then we differentiate the tracking error until control input v_{dr} and v_{qr} explicitly appeared, hence the input-output feedback linearization of (18) becomes

$$\begin{bmatrix} \ddot{e}_1 \\ \dot{e}_2 \end{bmatrix} = \begin{bmatrix} \phi_1 \\ \phi_2 \end{bmatrix} - \begin{bmatrix} \ddot{\omega}_{\mathrm{r\_ref}} \\ \dot{Q}_{\mathrm{s\_ref}} \end{bmatrix} + B \begin{bmatrix} v_{\mathrm{dr}} \\ v_{\mathrm{qr}} \end{bmatrix} \tag{19}$$

where

$$\begin{aligned} \phi_1 = {} & \tfrac{\dot{T}_{\mathrm{m}}}{2H_{\mathrm{m}}} - \tfrac{1}{2H_{\mathrm{m}}}\Big\{ w_{\mathrm{b}}\Big[\left(1 - \tfrac{\omega_{\mathrm{r}}}{\omega_{\mathrm{s}}}\right)\left(e'_{\mathrm{ds}} i_{\mathrm{qs}} - e'_{\mathrm{qs}} i_{\mathrm{ds}}\right) - \tfrac{1}{\omega_{\mathrm{s}} T_{\mathrm{r}}} \\ & \left(e'_{\mathrm{qs}} i_{\mathrm{qs}} + e'_{\mathrm{ds}} i_{\mathrm{ds}}\right)\Big] + \tfrac{\omega_{\mathrm{b}}}{\omega_{\mathrm{s}} L'_{\mathrm{s}}}\Big[\tfrac{\omega_{\mathrm{r}}}{\omega_{\mathrm{s}}}\left(e'^2_{\mathrm{ds}} + e'^2_{\mathrm{qs}}\right) \\ & + \omega_{\mathrm{s}} L'_{\mathrm{s}}(e'_{\mathrm{qs}} i_{\mathrm{ds}} - e'_{\mathrm{ds}} i_{\mathrm{qs}}) - R_1(e'_{\mathrm{qs}} i_{\mathrm{qs}} + e'_{\mathrm{ds}} i_{\mathrm{ds}}) \\ & - e'_{\mathrm{qs}} v_{\mathrm{qs}} - e'_{\mathrm{ds}} v_{\mathrm{ds}}\Big]\Big\} \end{aligned} \tag{20}$$

$$\begin{aligned} \phi_2 = {} & \tfrac{\omega_{\mathrm{b}}}{L'_{\mathrm{s}}}\left(\omega_{\mathrm{s}} L'_{\mathrm{s}} i_{\mathrm{qs}} + R_1 i_{\mathrm{ds}} - \tfrac{1}{\omega_{\mathrm{s}} T_{\mathrm{r}}} e'_{\mathrm{qs}} - \tfrac{\omega_{\mathrm{r}}}{\omega_{\mathrm{s}}} e'_{\mathrm{ds}}\right) v_{\mathrm{qs}} \\ & + \tfrac{\omega_{\mathrm{b}}}{L'_{\mathrm{s}}}\left(-R_1 i_{\mathrm{qs}} + \omega_{\mathrm{s}} L'_{\mathrm{s}} i_{\mathrm{ds}} + \tfrac{\omega_{\mathrm{r}}}{\omega_{\mathrm{s}}} e'_{\mathrm{qs}} - \tfrac{1}{\omega_{\mathrm{s}} T_{\mathrm{r}}} e'_{\mathrm{ds}} - v_{\mathrm{qs}}\right) v_{\mathrm{ds}} \end{aligned} \tag{21}$$

and

$$B = \begin{bmatrix} \frac{\omega_{\mathrm{b}} L_{\mathrm{m}}}{-2H_{\mathrm{m}} L_{\mathrm{rr}}}\left(\frac{e'_{\mathrm{ds}}}{\omega_{\mathrm{s}} L'_{\mathrm{s}}} - i_{\mathrm{qs}}\right) & \frac{\omega_{\mathrm{b}} L_{\mathrm{m}}}{-2H_{\mathrm{m}} L_{\mathrm{rr}}}\left(\frac{e'_{\mathrm{qs}}}{\omega_{\mathrm{s}} L'_{\mathrm{s}}} + i_{\mathrm{ds}}\right) \\ -\frac{\omega_{\mathrm{b}} L_{\mathrm{m}}}{L'_{\mathrm{s}} L_{\mathrm{rr}}} v_{\mathrm{qs}} & \frac{\omega_{\mathrm{b}} L_{\mathrm{m}}}{L'_{\mathrm{s}} L_{\mathrm{rr}}} v_{\mathrm{ds}} \end{bmatrix} \tag{22}$$

where B is the control gain matrix. As $det(B) = -\frac{\omega_{\rm b}^2 L_{\rm m}^2 v_{\rm qs}}{2H_{\rm m} L'_{\rm s} L_{\rm rr}^2}\left(\frac{e'_{\rm qs}}{\omega_{\rm s} L_{\rm s}} + i_{\rm ds}\right) \neq 0$, it is invertible and the transformed system is linearizable over the whole operation range.

The time derivative of $T_{\rm m}$ in (20) is

$$\dot{T}_{\rm m} = \frac{\partial T_{\rm m}}{\partial \omega_{\rm r}} \times \frac{d\omega_{\rm r}}{dt} + \frac{\partial T_{\rm m}}{\partial v_{\rm wind}} \times \frac{dv_{\rm wind}}{dt} \tag{23}$$

with

$$\begin{aligned}\frac{\partial T_{\rm m}}{\partial \omega_{\rm r}} =& \frac{1}{2}\rho A v_{\rm wind}^3 \Big\{ c_1 e^{-c_5\left(\frac{v_{\rm wind}}{R\omega_{\rm r}} - 0.035\right)} \Big[\frac{c_2 c_5 v_{\rm wind}^2}{R^2 \omega_{\rm r}^4} \\ & - \frac{(2c_2 + 0.035 c_2 c_5 + c_4 c_5) v_{\rm wind}}{R\omega_{\rm r}^3} \\ & + \frac{0.035 c_2 + c_4}{\omega_{\rm r}^2} \Big] \Big\}\end{aligned} \tag{24}$$

and

$$\begin{aligned}\frac{\partial T_{\rm m}}{\partial v_{\rm wind}} =& \frac{1}{2}\rho A v_{\rm wind}^2 \Big\{ c_1 e^{-c_5\left(\frac{v_{\rm wind}}{R\omega_{\rm r}} - 0.035\right)} \Big[- \frac{c_2 c_5 v_{\rm wind}^2}{R^2 \omega_{\rm r}^3} \\ & + \frac{(4c_2 + 0.035 c_2 c_5 + c_4 c_5) v_{\rm wind}}{R\omega_{\rm r}^2} \\ & - \frac{0.105 c_2 + 3 c_4}{\omega_{\rm r}} \Big] - \frac{2 c_6 R}{v_{\rm wind}} \Big\}\end{aligned} \tag{25}$$

where $\frac{d\omega_{\rm r}}{dt}$ is the acceleration rate of rotor speed and $\frac{dv_{\rm wind}}{dt}$ is the wind variation rate, respectively.

Let $v = [v_1 \quad v_2]^T$ be the new control input of the linearized system

$$\begin{bmatrix} \ddot{e}_1 \\ \dot{e}_2 \end{bmatrix} = \begin{bmatrix} v_1 \\ v_2 \end{bmatrix} = - \begin{bmatrix} \alpha_1 e_1 + \alpha_2 \dot{e}_1 \\ \alpha_3 e_2 \end{bmatrix} \tag{26}$$

where α_1, α_2, α_3 are the control gains. After choosing the appropriate gains α_i to make the above system be Hurwitz, i.e., all of its eigenvalues have negative real parts, the asymptotic error convergence would be ensured. To this end, we derive the nonlinear control law as

$$\begin{bmatrix} v_{\rm dr} \\ v_{\rm qr} \end{bmatrix} = B^{-1} \begin{bmatrix} -\phi_1 + \ddot{\omega}_{\rm r\_ref} + v_1 \\ -\phi_2 + \dot{Q}_{\rm s\_ref} + v_2 \end{bmatrix} \tag{27}$$

And the tracking error dynamics are

$$\begin{aligned} \ddot{e}_1 + \alpha_1 \dot{e}_1 + \alpha_2 e_1 = 0 \\ \dot{e}_2 + \alpha_3 e_2 = 0 \end{aligned} \tag{28}$$

From (27) one can find that the feedback linearization controller has an integrated structure. In essence it regulates the voltage injection of RSC to maintain the rotor speed $\omega_{\rm r}$ and reactive power $Q_{\rm s}$ to track their reference values.

C. The stability of internal dynamics

The internal dynamics of (19) correspond to $n - r$, here $n = 5$ is the order of the original system and $r = 3$ is the total relative degree respectively. The stability of internal dynamics can be analyzed by the zero-dynamic method in [17]. We set the tracking errors equal to zero $e_1 = e_2 = \dot{e}_1 = 0$, namely $Q_{\rm s} = Q_{\rm s\_ref}$, $\omega_{\rm r} = \omega_{\rm r\_ref}$ and $\dot{\omega}_{\rm r} = \dot{\omega}_{\rm r\_ref}$. Substitute these values into (5)-(10) it yields

$$\begin{aligned}\dot{e}'_{\rm qs} =& -\frac{\omega_{\rm s}^3 \omega_{\rm b} L'_{\rm s} (T_{\rm m\_ref} - 2H_{\rm m}\dot{\omega}_{\rm r\_ref})}{e'_{\rm qs}} + \omega_{\rm s}\omega_{\rm b} e'_{\rm ds} \\ \dot{e}'_{\rm ds} =& \frac{\omega_{\rm s}^2 \omega_{\rm b} (T_{\rm m\_ref} - 2H_{\rm m}\dot{\omega}_{\rm r\_ref})}{e'_{\rm qs}} \Big[\frac{\omega_{\rm s}^3 L'^2_{\rm s} (T_{\rm m\_ref} - 2H_{\rm m}\dot{\omega}_{\rm r\_ref})}{e'^2_{\rm qs}} \\ & - \frac{\omega_{\rm s} L'_{\rm s} e'_{\rm ds}}{e'_{\rm qs}} + R_1 - R_2 \Big] + \omega_{\rm s}\omega_{\rm b}(v_{\rm qs} - e'_{\rm qs})\end{aligned} \tag{29}$$

where

$$T_{\rm m\_ref} = \frac{\rho \pi R^3 C_{\rm p\_max} v_{\rm wind}^2}{2\lambda_{\rm opt}} \tag{30}$$

with

$$\dot{\omega}_{\rm r\_ref} = \frac{\lambda_{\rm opt}}{R}\dot{v}_{\rm wind} \tag{31}$$

We construct a Lyapunov function V for (29) as

$$V = \frac{1}{2}e'^2_{\rm qs} + \frac{1}{2}e'^2_{\rm ds} \tag{32}$$

Differentiating V along with the time obtains

$$\begin{aligned}\dot{V} =& e'_{\rm qs}\dot{e}'_{\rm qs} + e'_{\rm ds}\dot{e}'_{\rm ds} = \omega_{\rm s}^2 \omega_{\rm b}(T_{\rm m\_ref} - 2H_{\rm m}\dot{\omega}_{\rm r\_ref}) \Big[-\omega_{\rm s} L'_{\rm s} \\ & + \frac{\omega_{\rm s}^3 L'^2_{\rm s}(T_{\rm m\_ref} - 2H_{\rm m}\dot{\omega}_{\rm r\_ref}) e'_{\rm ds}}{e'^3_{\rm qs}} - \frac{\omega_{\rm s} L'_{\rm s} e'^2_{\rm ds}}{e'^2_{\rm qs}} \\ & + \frac{(R_1 - R_2) e'_{\rm ds}}{e'_{\rm qs}} \Big] + \omega_{\rm s}\omega_{\rm b} v_{\rm qs} e'_{\rm ds}\end{aligned} \tag{33}$$

The stability of (29) can then be determined by the sign of $\dot{V}$. We focus on the variable speed range $v_{\rm wind} = 8 - 12$ m/s, and the bounds of each variable are: $e'_{\rm qs} \in [1.002, 1.005]$ p.u., $e'_{\rm ds} \in [0.045, 0.098]$ p.u. and $T_{\rm m\_ref} \in [0.443, 0.996]$ p.u.. Assuming the wind variation rate is bounded as $|\dot{v}_{\rm wind}| \leq 1$ m/s it becomes

$$\begin{aligned}\dot{V} \leq \dot{V}_{\max} =& \omega_{\rm s}^2 \omega_{\rm b}(T_{\rm m\_ref\_max} - 2H_{\rm m}\dot{\omega}_{\rm r\_ref\_min}) \Big[-\omega_{\rm s} L'_{\rm s} + \\ & \frac{\omega_{\rm s}^3 L'^2_{\rm s}(T_{\rm m\_ref\_max} - 2H_{\rm m}\dot{\omega}_{\rm r\_ref\_min}) e'_{\rm ds\_max}}{e'^3_{\rm qs\_min}} - \\ & \frac{\omega_{\rm s} L'_{\rm s} e'^2_{\rm ds\_min}}{e'^2_{\rm qs\_max}} + \frac{(R_1 - R_2) e'_{\rm ds\_max}}{e'_{\rm qs\_min}} \Big] \\ & + \omega_{\rm s}\omega_{\rm b} v_{\rm s} e'_{\rm ds\_max} = -22.80 < 0\end{aligned} \tag{34}$$

Therefore (29) is asymptotically stable as $\dot{V} < 0$, and the stability of the linearized system (19) can be guaranteed.

IV. Modal Analysis and Simulation Study

We use both modal analysis and simulation study to verify the effectiveness of FLC. A 5 MW DFIG-WT is employed and the parameters can be found in the Appendix.

Modal analysis provides the system mode loci hence the system response under different operation condition can be studied. One can select sufficient operation points over the whole operation range, while the closed-loop system is linearized at each given operation point to form the Jacobian matrix. Table I gives the system modes under the nominal operation point ($v_{\rm wind} = 12$ m/s, $v_{\rm s} = 1.0$ p.u.). The $\lambda_{1,2}$, $\lambda_{3,4}$ and

λ_5 are the current, voltage and mechanical mode respectively. $\lambda_i = \sigma_i \pm j\omega_i$, where the stability is determined by the sign of σ_i, and ω_i is the natural frequency of oscillations. The original system (5)-(10) has been transformed into the equivalent linear system (19) and the internal dynamics (29). The former corresponds to the current and mechanical mode of ($i_{\rm qs}$, $i_{\rm ds}$ $\omega_{\rm r}$), and the latter corresponds to the voltage mode of ($e'_{\rm qs}$, $e'_{\rm ds}$). It is worth to note that $\lambda_{1,2}$ are fully decoupled without imaginary part in FLC, although the close location of $\lambda_{3,4}$ to the imaginary axis decreases the stability margin, their stability is guaranteed by (34), and more damping can be provided in λ_5.

A. Maximum power point tracking (MPPT) performance

Simulation study for an increase in wind speed from 8 m/s and 12 m/s is showed in Fig. 2(a). The rotor speed and conversion coefficient are given in Fig. 2(b)-(c). It shows that more accurate tracking and faster restoration of conversion coefficient can be achieved by FLC against VC over the whole operation range.

The corresponding system mode loci is presented in Fig. 3. One can find that $i_{\rm qs}$, $e'_{\rm qs}$ and $e'_{\rm ds}$ modes of FLC only vary slightly such that the operation performance is maintained as wind speed changes, and the $i_{\rm ds}$ mode is invariant regardless of the operation condition, which demonstrates a fully decoupled reactive power regulation from rotor speed control, and more damping can be provided as the $\omega_{\rm r}$ mode locates further from imaginary axis. In fact, the dramatic modes variation of VC is attributed to the system nonlinearity, which has been fully removed by FLC thus a global optimal control performance over the variable speed range can be achieved.

In order to verify the results of modal analysis, simulation study is carried out to illustrate the system responses in Fig. 4. Because the control inputs (rotor voltage $v_{\rm qr}$ and $v_{\rm dr}$) may exceed the admissible capacity of RSC at some operation point, their values must be limited. Here $v_{\rm dr}$ and $v_{\rm qr}$ are scaled proportionally as: if $v_{\rm r} = \sqrt{v_{\rm dr}^2 + v_{\rm qr}^2} > v_{\rm r\_max}$, then we set $v_{\rm dr\_lim} = v_{\rm dr} v_{\rm r\_max}/v_{\rm r}$ and $v_{\rm qr\_lim} = v_{\rm qr} v_{\rm r\_max}/v_{\rm r}$, respectively.

During the wind variation the net power output $P_{\rm a} = P_{\rm m} - P_{\rm e} > 0$ must be satisfied to produce an accelerating torque as wind speed increases, however, due to the mechanical constraint $P_{\rm m}$ could not adjust immediately hence a temporary drop in $P_{\rm e}$ has to be compromised. It shows from Fig. 4 that a smoother active power tracking and fully decoupled reactive power regulation can be achieved by FLC with less control cost.

B. Low-voltage ride-through (LVRT) capability

With the unprecedented increasing integration of wind generators into grid, it is required the DFIG-WT to be capable of LVRT when the voltage is temporarily reduced due to a fault or load change in the grid, or even addresses the generator to stay operational and not disconnect from the grid during and after the voltage dip.

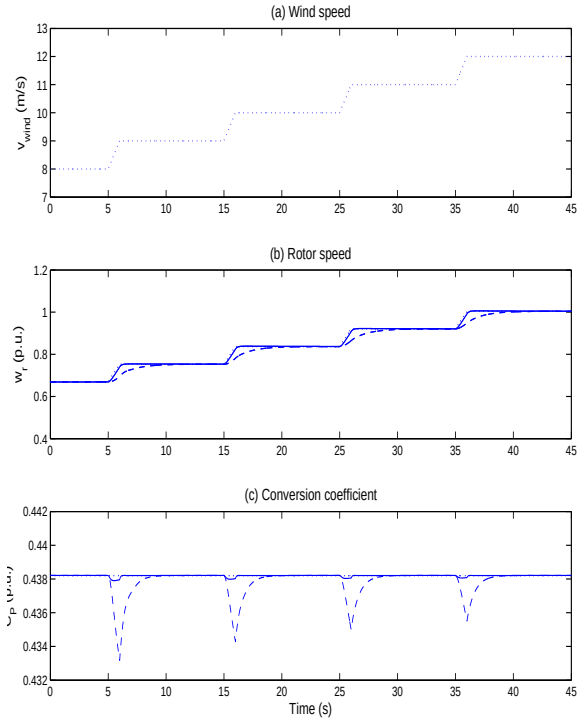

Fig. 2. MPPT performance, dotted line: reference value, dashed line: VC, solid line: FLC.

TABLE I
SYSTEM MODE UNDER NOMINAL OPERATION POINT

poles	system modes	VC	FLC
λ_1	$i_{\rm qs}$	$-2.33 + j25.42$	-16.2
λ_2	$i_{\rm ds}$	$-2.33 - j25.42$	-8
λ_3	$e'_{\rm qs}$	$-11.20 + j310$	$-1.85 + j314.8$
λ_4	$e'_{\rm ds}$	$-11.20 - j310$	$-1.85 - j314.8$
λ_5	$\omega_{\rm r}$	-0.27	-1.07

The system loci of $v_{\rm s} = 0.2 - 1.0$ p.u. is showed in Fig. 5, a dramatic variation of VC system modes can be found, while FLC system modes are insensitive to the voltage dip thus its LVRT capability is enhanced. A 625 ms voltage dip to 0.2 p.u. and restores to 0.9 p.u. is simulated in Fig. 6 with a total fault time of 3 s. In VC the significant variation of active power might cause the activation of the protective devices to disconnect the generator from the grid, the external reactive power compensation is required for the purpose of reactive power regulation as well. In contrast FLC can eliminate the effect of grid fault smoothly and rapidly, therefore improve the system LVRT capacity.

C. Fully decoupled control

The decoupled control of VC is derived from the assumption of constant stator flux or stator voltage, this is no longer true when fault occurs in the grid, however FLC can achieve the fully decoupled control as no such assumption is made. The system responses with a simultaneous 30% voltage dip and 1 m/s wind speed decrease from the nominal operation point

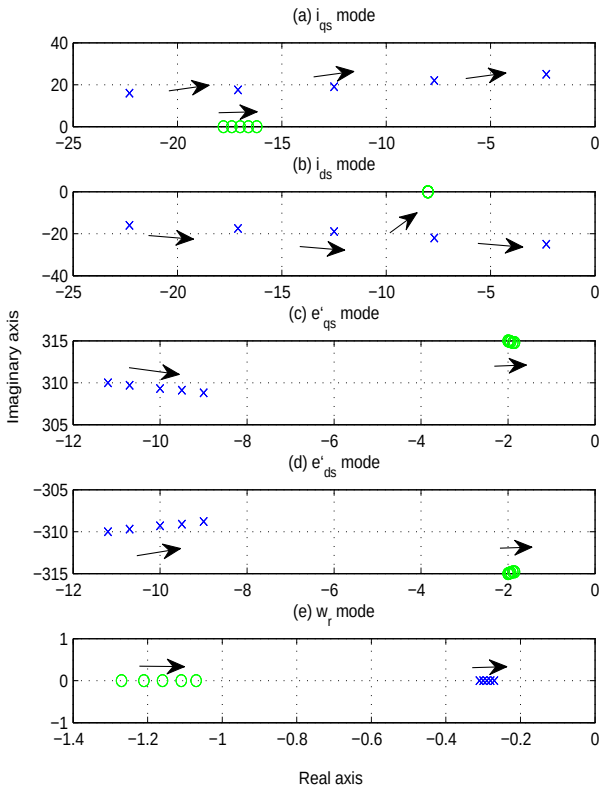

Fig. 3. System mode loci with $v_{\text{wind}} = 8 - 12$ m/s, $\times$: VC, $\circ$: FLC.

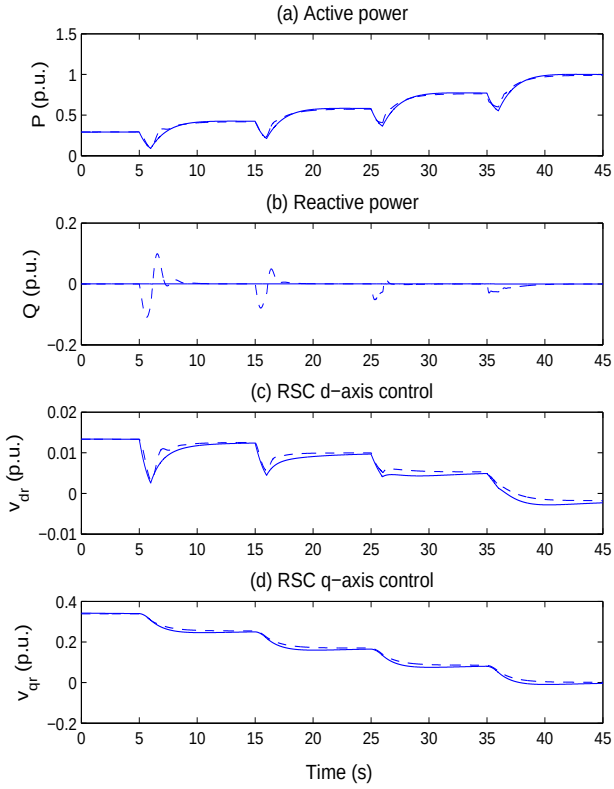

Fig. 4. System responses in MPPT, dashed line: VC, solid line: FLC.

is showed in Fig. 7. It shows that the performance of active power control in VC degrades during fault, while FLC can effectively control the active power and regulate the reactive power as its reference value.

D. System robustness with parameter uncertainty

It is important to mention that the effect of system sensitivity to parameter uncertainty may be particularly severe when the linearizing transformation is poorly conditioned. Since the accurate system parameter is not accessible in practice, it can have strong adverse effects on FLC performance which does not guarantee robustness in theory.

To address this issue Fig. 8 illustrates the system mode loci as the stator resistance varies $2.0R_{\text{s\_nom}} \geq R_{\text{s}} \geq R_{\text{s\_nom}}$, which is a common result from generator heating. Note that the stability margin of i_{qs} mode and internal dynamics decreases dramatically, hence its control performance will degrade as stator resistance varied. However, none of the system parameter is used in VC design it is robust to parameter uncertainty. Fig. 9 shows the simulation results with $R_{\text{s}} = 1.0R_{\text{s\_nom}}$, $R_{\text{s}} = 1.5R_{\text{s\_nom}}$ and $R_{\text{s}} = 2.0R_{\text{s\_nom}}$ respectively, it shows the feedback linearization controller provides incorrect control input and can no longer drive the active and reactive power to their reference value, consequently it is vulnerable in terms of parameter uncertainties.

V. Conclusion

We have designed a feedback linearization controller to achieve MPPT in this paper, which fully removes the system nonlinearity to obtain a global optimal control. Based on the detailed DFIG-WT the stator dynamics is taken into account hence system transient dynamics is included. The original system is transformed into the external and internal dynamics respectively, desired control goal is achieved by imposing the it on the external dynamics via exact input-output linearization, meanwhile the asymptotic stability of the internal dynamics is proved in the context of Lyapunov.

Modal analysis shows that each mode of FLC varies slightly under different operation conditions, thus the global optimal control is obtained. Furthermore, the LVRT capacity of system is also significantly enhanced as the nonlinearity has been removed. As none of the model assumption is made fully decoupled control is achieved. However, the effectiveness of the approach requires accurate model which is difficult to acquire in practice, simulation studies show the control performance degrades dramatically in the face of stator resistance uncertainties. Considerable more work in future, hopefully, will be done in designing the nonlinear robust and adaptive controllers to resolve this issue.

Appendix

System parameters [8]:

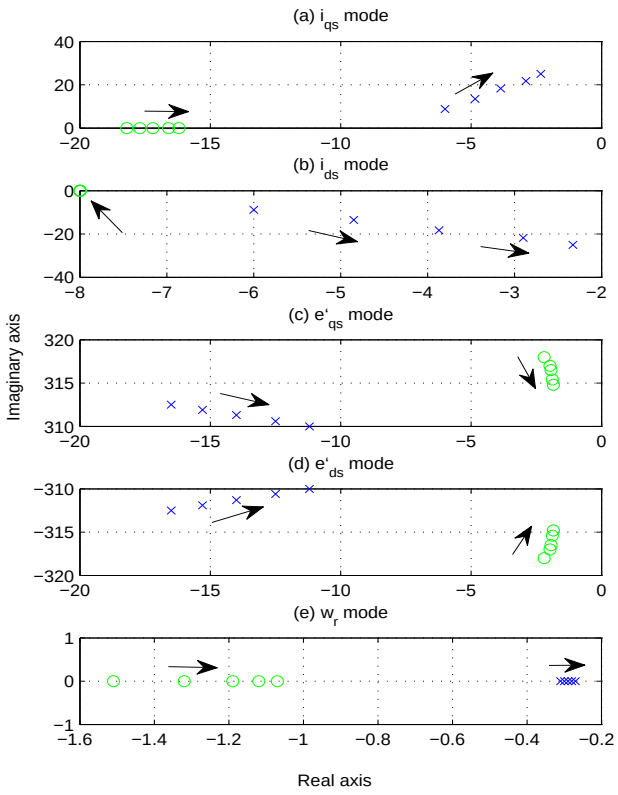

Fig. 5. System mode loci with $v_{\rm s} = 0.2 - 1.0$ p.u., $\times$: VC, $\circ$: FLC.

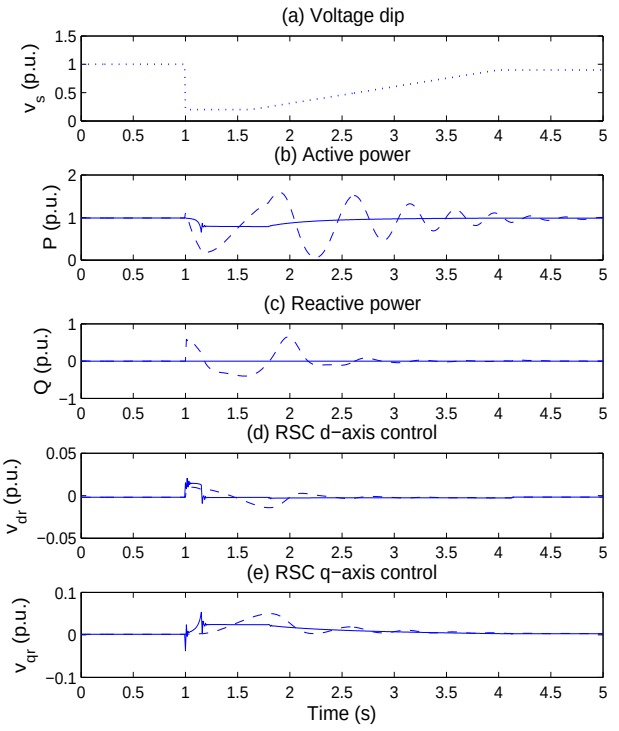

Fig. 6. System responses in LVRT, dashed line: VC, solid line: FLC.

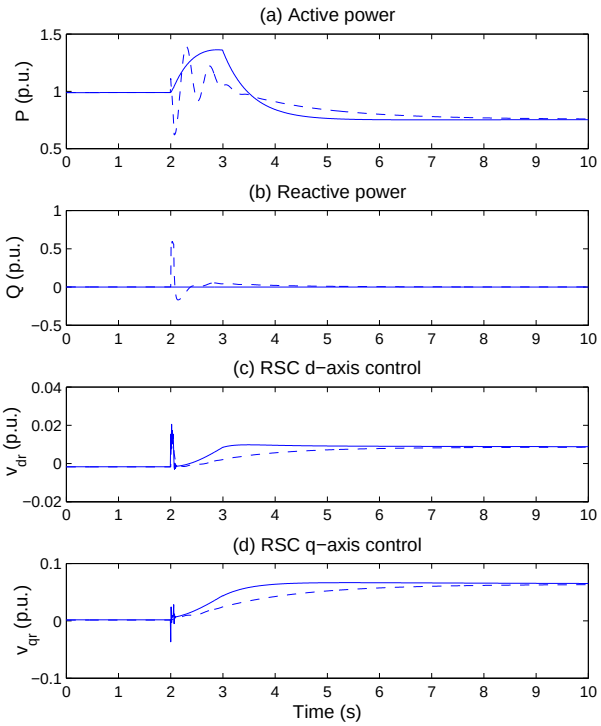

Fig. 7. System responses with simultaneous 30% voltage dip and 1m/s wind speed decrease from the nominal point, dashed line: VC, solid line: FLC.

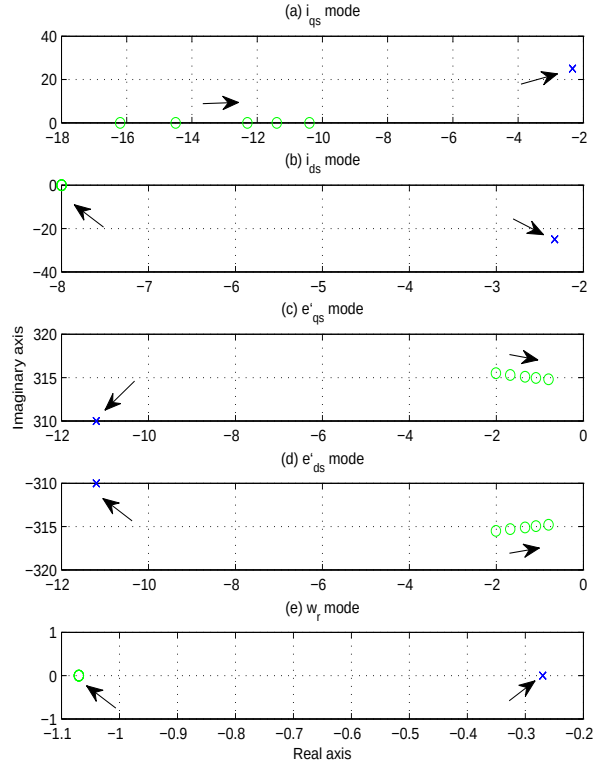

Fig. 8. System mode loci with $R_{\rm s} = 1.0 - 2.0 R_{\rm s\_nom}$, $\times$: VC, $\circ$: FLC.

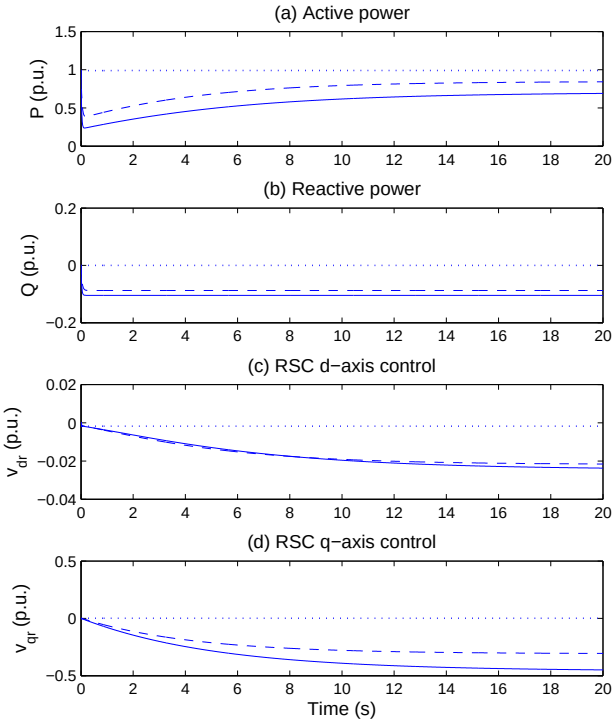

Fig. 9. System response with parameter uncertainty, dotted line: $R_{\rm s} = 1.0R_{\rm s\_nom}$, dashed line: $R_{\rm s} = 1.5R_{\rm s\_nom}$, solid line: $R_{\rm s} = 2.0R_{\rm s\_nom}$.

$\omega_{\rm b} = 100\pi$ rad/s, $\omega_{\rm s} = 1.0$ p.u., $\omega_{\rm r\_base} = 1.29$, $v_{\rm s\_nom} = 1.0$ p.u..

DFIG parameters:

$P_{\rm rated} = 5$ MW, $R_{\rm s} = 0.005$ p.u., $R_{\rm r} = 1.1R_{\rm s}$, $L_{\rm m} = 4.0$ p.u., $L_{\rm ss} = 1.01L_{\rm m}$, $L_{\rm rr} = 1.005L_{\rm ss}$.

Wind turbine parameters:

$\rho = 1.225$ Kg/m^3, $R = 58.59$ m^2, $v_{\rm wind\_nom} = 12$ m/s, $\lambda_{\rm opt} = 6.325$, $H_{\rm m} = 4.4$ s, $D = 0$ p.u..

REFERENCES

[1] M. Tazil, V. Kumar, R. C. Bansal, S. Kong, Z. Y. Dong, W. Freitas and H. D. Mathur, "Three-phase doubly fed induction generators: an overview," *IET Electric Power Applications*, vol. 4, no. 2, pp. 75-89, 2010.

[2] C. W. Luen and H. Y. Yih, "Controller design for an induction generator driven by a variable-speed wind turbine," *IEEE Trans. Energy Convers.*, vol. 21, no. 3, pp. 625-635, Jun. 2006.

[3] A. Tapia, G. Tapia, J. X. Ostolaza and J. R. Saenz, "Modeling and control of a wind turbine driven doubly fed induction generator," *IEEE Trans. Energy Convers.*, vol. 18, no. 2, pp. 194-204, Jun. 2003.

[4] R. Pena, J. C. Clare and G. M. Asher, "Doubly fed induction generator using back-to-back PWM converters and its application to variable speed wind-energy generation," *IEEE Proc Electrical Power Applications*, vol. 143, no. 3, pp. 231-241, May 1996.

[5] R. Cardenas and R. Pena, "Sensorless vector control of induction machines for variable-speed wind energy applications," *IEEE Trans. Energy Convers.*, vol. 19, no. 1, pp. 196-205, Mar. 2004.

[6] S. Y. Shao, E. Abdi, F. Barati and R. Mcmahon, "Stator-flux-oriented vector vontrol for brushless doubly fed induction generator," *IEEE Trans. Ind. Electron.*, vol. 56, no. 10, pp. 4220-4228, Oct. 2009.

[7] S. H. Li, T. A. Haskew, K. A. Williams and R. P. Swatloski, "Control of DFIG wind turbine with direct-current vector control configuration," *IEEE Trans. on Sustainable Energy*, pp. 1-11, Jan. 2012.

[8] M. Fei and B. Pal, "Modal analysis of grid-connected doubly fed induction generators," *IEEE Trans. Energy Convers.*, vol. 22, no. 3, pp. 728-736, Sept. 2007.

[9] L. H. Yang, Z. Xu, J. Ostergaard, Z. Y. Dong, K. P. Wong and X. K. Ma, "Oscillatory stability and eigenvalue sensitivity analysis of a DFIG wind turbine system," *IEEE Trans. Energy Convers.*, vol. 26, no. 1, pp. 328-339, Nov. 2011.

[10] F. Wu, X. P. Zhang, K. Godfrey and P. Ju, "Small signal stability analysis and optimal control of a wind turbine with doubly fed induction generator," *IET Gener. Transm. Distrib.*, vol. 1, no. 5, pp. 751-760, Nov. 2007.

[11] B. Boukhezzar and H. Siguerdidjane, "Nonlinear control of a variable-speed wind turbine using a two-mass model," in *IEEE Trans. Energy Convers.*, vol. 26, no. 1, pp. 149-162, Mar. 2011.

[12] B. Beltran, T. A. Ali and M. H. Benbouzid, "Sliding mode power control of variable-speed wind energy conversion systems," *IEEE Trans. Energy Convers.*, vol. 23, no.2, pp. 551-558, Jun. 2008.

[13] A. Khedher, N. Khemiri and M. F. Mimouni, "Wind energy conversion system using DFIG controlled by backstepping and sliding mode strategies," *International Journal of Renewable Energy Research (IJRER).*, vol. 2, no. 3, pp. 421-430, 2012.

[14] D. C. Lee, "DC-bus voltage control of three-phase AC/DC PWM converters using feedback linearization," *IEEE Trans. Ind. Appl.*, vol. 36, no. 3, pp. 826-833, Jun. 2000.

[15] F. Wu and X. P. Zhang, "Decentralized nonlinear control of wind turbine with doubly fed induction generator," *IEEE Trans. Power Syst.*, vol. 23, no. 2, pp. 613-621, May 2008.

[16] J. M. Mauricio, A. E. Leon, A. Gomez-Exposito and J. A. Solsona, "An adaptive nonlinear controller for DFIM-based wind energy conversion system," *IEEE Trans. Energy Convers.*, vol. 23, no. 4, pp. 1025-1035, Dec. 2010.

[17] H. K. Khalil, *Nonlinear Systems.* NJ, 2002, 3rd edn.

[18] W. Qiao, "Dynamic modeling and control of doubly fed induction generators driven by wind turbines," *Power Systems Conference and Exposition*, pp. 1-8, 2009.

[19] L. Yazhou, A. Mullane, G. Ightbody, and R. Yacamini, "Modeling of the wind turbine with a doubly fed induction generator for grid integration studies," *IEEE Trans. Energy Convers.*, vol. 21, no. 1, pp. 257-264, Mar. 2006.

[20] T. Ackerman, "Wind Power in Power Systems,," *New York: Wiley.*, 2005.

[21] K. Takaaki, T. Yuji, K. Hirotoshi, K. Daichi, Tanaka and Akio, "Power smoothing and MPPT for grid-connected wind power generation with doubly fed induction generator," *IEEJ Trans. on Power and Energy*, vol. 128, pp. 7, pp. 937-944, 2008.

[22] V. Galdi, A. Piccolo, and P. Siano, "Designing an adaptive fuzzy controller for maximum wind energy extraction," *IEEE Trans. Energy Convers.*, vol. 23, no. 2, pp. 559-569, Jun. 2008.

[23] D. Xiang, L. Ran, P. J. Tavner, and S. Yang, "Control of a doubly fed induction generator in a wind turbine during grid fault ride-through," *IEEE Trans. Energy Convers.*, vol. 21, no. 3, pp. 652-662, Sept. 2006.

[24] M. Rahimi and M. Parniani, "Transient performance improvement of wind turbines with doubly fed induction generators using nonlinear control strategy," *IEEE Trans. Energy Convers.*, vol. 25, no. 2, pp. 514-525, Jun. 2010.

[25] L. Jiang, Q. H. Wu, J. Wang, C. Zhang and X. X. Zhou, "Robust observer-based nonlinear control of multimachine power systems," *IEE Proceedings, Gener. Transm. Distrib.*, vol. 148, no. 6, pp. 623-631, Nov. 2001.